Title

Acid-Stable Peroxoniobophosphate Clusters To Make Patterned Films

Journal

Chemistry - A European Journal, 21(18)

ISSN

0947-6539

Authors

Son, Jung-Ho
Park, Deok-Hie
Keszler, Douglas A
et al.

Publication Date

2015-04-27

DOI

10.1002/chem.201500684

Peer reviewed

ChemPubSoc Europe

DOI: 10.1002/chem.201500684

CHEMISTRY
A European Journal
Communication

Polyoxometalates

Acid-Stable Peroxoniobophosphate Clusters To Make Patterned Films

Jung-Ho Son,*[a] Deok-Hie Park,[b] Douglas A. Keszler,[b] and William H. Casey[a, c]

Abstract: Two new peroxoniobophosphate clusters were isolated as tetramethylammonium (TMA) salts having the stoichiometries: $TMA_5[HNb_4P_2O_{14}(O_2)_4]\cdot 9H_2O$ and $TMA_3[H_7Nb_6P_4O_{24}(O_2)_6]\cdot 7H_2O$. The former is stable over the pH range: $3 < pH < 12$ and the latter is stable only below pH 3. These two molecules interconvert as a function of solution pH. The $[H_7Nb_6P_4O_{24}(O_2)_6]^{3-}$ cluster can be used to fabricate patterned niobium phosphate films by electron-beam lithography after solution deposition.

Aqueous metal-oxide clusters are interesting as potential molecular precursors for fabricating large-area films and for making nanopatterned oxide structures with features at the level of single-digit nanometers. Such advances would help enable continued adherence to Moore's Law in next-generation semiconductor manufacturing. Some existing examples of solution-processed and patterned films include SiO_2 from hydrogen silsesquioxane (HSQ),[1] SnO_2,[2] Al_2O_3, TiO_2,[3] ZrO_2, and HfO_2.[4] The solutions in all of these cases contain an oxide cluster that is thought to serve as a precursor to the film. For example, films, formed from peroxo-hafnium-sulfate (HafSOx) precursor solutions, can be lithographically patterned to produce dense HfO_2 nanostructures at resolutions near 10 nm.[5] The environmental impact of this method is anticipated to be much less than conventional methods because of the reduction in both resist waste and the number of process steps. The cluster species in the HafSOx solutions are apparently mixed oligomers of uncertain stoichiometry.[6]

Here we advance the field by showing that peroxoniobophosphate clusters can generate patternable niobium phosphate thin films. Moreover, we have explored the chemistry of peroxoniobate clusters that incorporate phosphate to expand the pH stability range of the niobate clusters to the acidic region. Polyoxoniobate clusters are generally only stable under neutral to basic conditions. Since peroxoniobate clusters have more surface atoms than non-peroxo analogues, and thus lower surface charge density, the former will exhibit lower basicity and thus peroxo substitution might extend the pH range of stability. Phosphate groups can add acidic functionality and solubility. We note that polyoxotungstates substituted with peroxoniobate groups show wide pH stabilities, due to the coexistence of acidic tungstate and basic niobate.[7] Niobium phosphate glasses also have been of industrial interest for optical applications and as a nuclear waste host.[8] Niobates and tantalates are known to form various peroxo complexes, and these find use as oxidation catalysts for organic reactions and precursors for metal-oxide films.[9] Peroxoniobates have also been studied for their possible anticancer activity.[10] Peroxoniobate clusters have been recently synthesized and characterized, such as peroxo-Nb_6 and peroxo-$Ti_{12}Nb_6$ clusters.[11,12] More recently, a peroxonioboarsenate $Cs_{2.5}H_{1.5}Na_2[Nb_4As_2O_{14}(O_2)_4]$ (Nb_4As_2) cluster has been reported,[13] and its structure is similar to one of the peroxoniobophosphate clusters described in this paper.

Here we report the synthesis and characterization of two peroxoniobophosphate clusters as TMA (tetramethylammonium) salts, $TMA_5[HNb_4P_2O_{14}(O_2)_4]\cdot 9H_2O$ (**1**, Nb_4P_2) and $TMA_3[H_7Nb_6P_4O_{24}(O_2)_6]\cdot 7H_2O$ (**2**, Nb_6P_4), and demonstrate that atomically smooth, patterned, oxide films can be fabricated by using the Nb_6P_4 cluster as precursor. These two chemically and structurally related clusters are inter-convertible by suitable choice of the solution conditions.

The compounds **1** and **2** can be synthesized at room temperature by simple mixing of a niobate-cluster solution, hydrogen peroxide, and phosphoric acid. First, a TMA salt of decaniobate or hexaniobate is dissolved in water with stirring. Adding excess hydrogen peroxide leads to formation of peroxo-Nb_6 ions within a few minutes.[11] After most of the bubbles that arise from excess H_2O_2 cease evolving, phosphoric acid is added. Both the initial pH of the original niobate solution and the amount of phosphoric acid, thus the final pH, determines whether **1** or **2** form. Generally **1** forms at solution $pH > 3$, and **2** forms only at low pH; ($pH < 3$). The solution comprising mostly **1** at high pH is nearly colorless, whereas the solution at $pH < 3$ is intensely yellow. Another viable synthetic route is achieved by adding hydrogen peroxide at room temperature to a hydrothermally reacted solution of hydrous niobium oxide, TMAOH, and phosphoric acid.

The structure of Nb_4P_2 is similar to that of Nb_4As_2,[13] with two phosphate ligands stabilizing the peroxo-Nb_4 core

[a] Dr. J.-H. Son, Prof. W. H. Casey
Department of Chemistry, University of California, Davis
One Shields Ave, Davis, CA 95616 (USA)
Fax: (+1) 530-752-8995
E-mail: junghoson@gmail.com

[b] D.-H. Park, Prof. D. A. Keszler
Department of Chemistry, 153 Gilbert Hall, Oregon State University
Corvallis, OR 97331-4003 (USA)

[c] Prof. W. H. Casey
Department of Earth and Planetary Science
One Shields Ave, Davis, CA 95616 (USA)

Supporting information for this article is available on the WWW under http://dx.doi.org/10.1002/chem.201500684.

(Figure 1). Overall, the structures of these clusters are similar to those of the peroxo-Nb_6 cluster.[11] Two phosphate groups are substituted for two adjacent Nb^V sites in peroxo-Nb_6, thereby reducing the binding of the central oxygen from μ_6 to μ_4

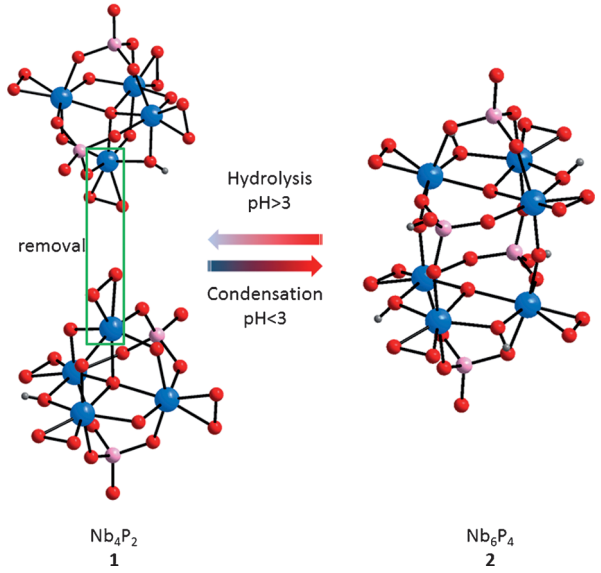

Figure 1. Reversible association and dissociation of Nb_4P_2 and Nb_6P_4. (Nb: blue; O: red; P: pink; H: gray).

(Figure 1). During the final crystal structure refinement cycles, a proton was found on the surface of the cluster from the electron density map. The proton is located at one of Nb-μ_2-O-Nb units, thus the formula of the cluster is represented as $[HNb_4P_2O_{14}(O_2)_4]^{5-}$. The charge of the Nb_4P_2 cluster is balanced by five TMA ions in the crystal structure.

The structure of Nb_6P_4 is related to that of Nb_4P_2, in a way that it can form by condensation of two Nb_4P_2 units, with loss of one corner Nb(O_2) site from each (Figure 1). The structure of Nb_6P_4 can be viewed as two thus-formed Nb_3P_2 units condensed via two Nb-μ_2-O-Nb and two P-μ_2-O-Nb bridges. The structure of Nb_6P_4 possesses two μ_3-O units at the center of Nb_3P_2 subunits. The structure of Nb_6P_4 exhibits a high degree of protonation, as expected from its low-pH synthesis conditions and relatively high proton affinities. Four Nb-μ_2-O-Nb units within the two Nb_3P_2 subunits are protonated in the Nb_6P_4 cluster, as found in the electron density map. The linking Nb-μ_2-O-Nb and Nb-μ_2-O-P units between the Nb_3P_2 units are not protonated. The terminal oxygen atoms of two equatorial phosphate groups are protonated; these can be regarded as P-OH groups. Additionally, one of the axial phosphate groups is protonated and the clusters are linked by this proton via hydrogen bonding to form one-dimensional chains along [010] and [1−10] directions. These protons attached to phosphates were also found in the electron density map. The seven bound protons and three TMA countercations balance the charge of the $[Nb_6P_4O_{24}(O_2)_6]^{10-}$ cluster. The pH of the 15 mM solution of Nb_6P_4 is approximately 2.0, thus the Nb_6P_4 cluster behaves more like traditional Mo- or W-based heteropoly acids, but differs distinctly from most of other polyoxoniobate clusters, which are stable at neutral to basic pH conditions. Most notably compound **2** is soluble in distilled water up to 0.02 M, and **1** is very soluble in water, making processing of it environmentally benign.

Selected ^{31}P MAS-NMR spectra of **1** and **2** are shown in Figure 2. The ^{31}P NMR spectrum for an amorphous sample of **1** exhibits a single peak at $\delta = -2.2$ ppm that splits into two resolvable peaks at $\delta = 0.2$ and -2.7 ppm when the material is fully crystalline. Two sites of nearly equal intensity are expected

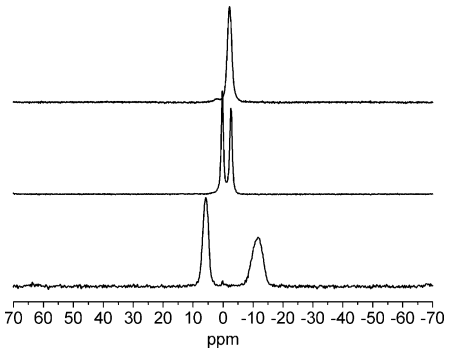

Figure 2. ^{31}P MAS NMR spectra of **1** (amorphous, top), **1** (crystalline, middle) and **2** (bottom).

from the two nonequivalent phosphate groups in the structure. Although the two phosphate groups are equivalent within Nb_4P_2 due to its C_{2v} symmetry, they have different outer environments—one phosphate has two hydrogen-bonded waters, whereas the other phosphate has three hydrogen-bonded waters. In the spectra of **2**, two different peaks are observed, and we assign the sharper peak at $\delta = 5.7$ ppm to an axial phosphate, and the broader peak at $\delta = -11.7$ ppm to an equatorial phosphate because the axial phosphates have a smaller variation in P–O distances (1.525(3)–1.550(2) Å) compared with those of the bridging equatorial phosphate (1.508(2)–1.561(2) Å). In the solution, **1** exhibits a single peak at $\delta = 1.7$ ppm, and **2** exhibits two peaks at $\delta = 7.0$ and -10.1 ppm (see Figure S2 in the Supporting Information), which agree with ^{31}P MAS NMR data.

In addition, ^1H MAS-NMR spectra were collected to characterize the environments of the protons bound to the clusters (Figure 3). For both clusters **1** and **2**, a conspicuous large peak arising from the TMA ions is observed near $\delta = 3.5$ ppm; peaks associated with waters of crystallization are observed at $\delta = 4.6$ and 5.6 ppm for **1** and **2**, respectively. Both compounds feature additional downfield peaks at $\delta = 7.5$ ppm (**1**) and $\delta = 8.6$ ppm (**2**), which we assign as protons bound to Nb-μ_2-O-Nb. ^1H MAS NMR spectra of protonated hexaniobate clusters at the bridging Nb-μ_2-O-Nb unit exhibit ^1H peaks either at 1 ppm or between 8 and 10 ppm, depending upon subtle differences in the outer environment and the countercations.[14] We assume that the inclusion of phosphate groups, and thus the more acidic character of **1** and **2**, is responsible for the downfield shifts of the Nb-μ_2-O-Nb bound proton peaks. A distinct peak at $\delta = 14.8$ ppm is observed in the ^1H MAS-NMR spectra of **2**, which is assigned to the acidic protons attached to the phos-

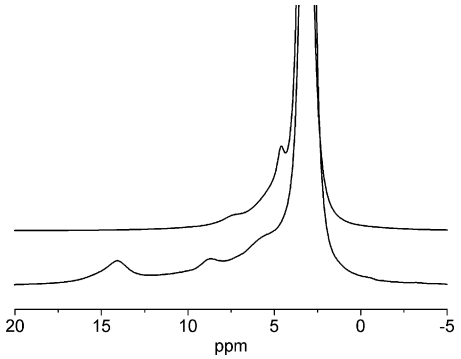

Figure 3. ^{1}H MAS NMR spectra of **1** (top) and **2** (bottom).

phate groups. This feature is absent in the spectra of **1**, which agrees with the crystal structures.

Raman spectra of **1**, **2**, and the unsubstituted peroxo-Nb_6 cluster are given in Figure 4. Signals from ν_s(O–O) are clearly seen in the range 800–900 cm^{-1} with stronger ν_s(M–O_2) peaks located between 500 and 700 cm^{-1}.[9] A single ν_s(O–O) peak is observed for peroxo-Nb_6, whereas split peaks are observed for Nb_4P_2 and Nb_6P_4. From the crystal structure, the peroxo groups

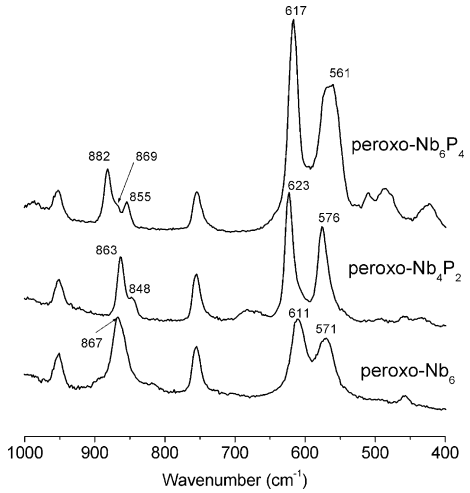

Figure 4. Raman spectra of **1**, **2** and peroxo-Nb_6.

in the peroxo-Nb_6 cluster are known to be chemically identical. In **1** (Figure 1), only two faces of the distorted Nb_4 core are capped by phosphate groups. The capping effectively produces chemically distinct peroxo environments. In **2**, the peroxo groups are approximately aligned in the planes of the two Nb_3 triangles. The asymmetric nature of the phosphate bridging between these triangular moieties (Figure 1), however, leads to chemical nonequivalence of the peroxo groups, as evidenced by the split peaks in the Raman spectrum. FT-IR spectra (Figure S3) of **1** and **2** exhibit a number of phosphate bands between 1000 and 1200 cm^{-1}, and **2** exhibits more phosphate bands, consistent with the two chemically and structurally distinct phosphates in Nb_6P_4. The ν_{as}(O–O) bands near 850 cm^{-1} in the FT-IR spectra are split for **1** and **2** similarly to the Raman data, and **2** shows a larger split between the ν_{as}(O–O) bands.

To better understand the formation of these new clusters, their interconversion was monitored as a function of time or pH by using ESI-MS. First, the formation of Nb_4P_2 or Nb_6P_4 was monitored after adding controlled amounts of phosphoric acid to the solution of the peroxo-Nb_6 cluster (see Figure S4 and S5). When the Nb:P ratio was 1:0.5, only Nb_4P_2 clusters formed (pH 3.8) and the solution remained nearly colorless. When excess phosphoric acid was added to make the Nb:P ratio 1:1.25 (pH 2.2), the Nb_6P_4 clusters formed and the solution color changed to yellow. When an intermediate amount of phosphoric acid was added, a mixture of Nb_4P_2 and Nb_6P_4 formed. The complete formation of Nb_4P_2 or Nb_6P_4 took about one day at room temperature.

Conversion of Nb_6P_4 to Nb_4P_2 was studied by addition of TMAOH to an Nb_6P_4 solution. The Nb_6P_4 cluster has seven protons attached to the surface oxygen atoms, thus we prepared seven different Nb_6P_4 solutions, comprising one to seven equivalents of TMAOH (Figure 5). Each solution was monitored by ESI-MS as a function of time (Figure S6). Although the color change was instant, actual conversion of **2** to **1** was slower. For example, the solution of **2** with seven equivalents of TMAOH completely converted to **1** within a day, and the solution of **2** with six equivalents of TMAOH nearly converted to **1** only after 3 days. All of the solutions containing one to seven equivalents of TMAOH converted to **1** after a few weeks, and all solutions became nearly colorless except the solutions with one or two equivalents of TMAOH. This indicates that pH is the determining factor in the hydrolysis of Nb_6P_4 to Nb_4P_2,

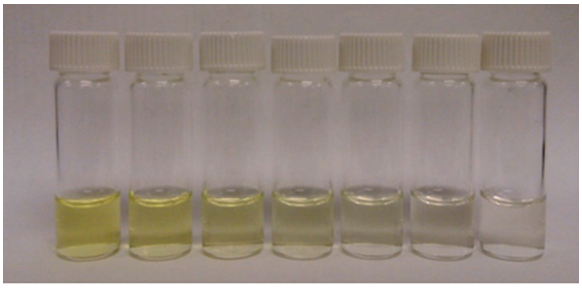

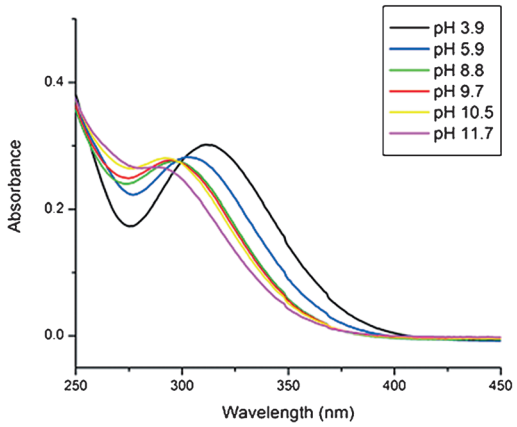

Figure 5. The photograph (top) is of a 15 mM solution of **2** with varying amounts of TMAOH added: 1 equiv (far left) to 7 equiv (far right) and UV/Vis spectra (bottom) of a 0.04 mM solution of **2** in 0.1 M TMACl solution, during titration with TMAOH solution.

not the amount of base equivalent added. The conversion of **2** to **1** is nearly quantitative, as indicated by peak intensities in the ESI-MS spectra of the solutions.

The Nb_4P_2 cluster is kinetically stable across a broad range of pH (3–12), as determined by pH-dependent ESI-MS (Figure S7), and this point is important for its industrial uses. This wide stability range of Nb_4P_2 is interesting because most of the known polyoxoniobates form insoluble amorphous niobium-oxide precipitate when the pH is lowered below 4. The wide stability of Nb_4P_2 is distinct when compared to peroxo-Nb_6, which is only stable in the range $6 < pH < 12$. When phosphoric acid was added to lower the pH of the Nb_4P_2 solution below 3, the colorless solution changed to yellow immediately, which is the characteristic color of Nb_6P_4. From ESI-MS, Nb_4P_2 completely condenses to Nb_6P_4 at pH < 2.5 within one hour after addition of phosphoric acid (Figure S8). We note that the conversion of Nb_4P_2 to Nb_6P_4 is faster (~1 hour) than other inter-cluster conversion processes discussed above (~1 day). When HCl was added to Nb_4P_2 solution to lower the pH instead of phosphoric acid, ESI-MS peak intensities of newly formed Nb_6P_4 are lower than those of the solution where phosphoric acid was added. Thus not only is pH the determining factor for complete conversion of Nb_4P_2 to Nb_6P_4, but excess phosphoric acid is required. This excess is partly understandable because each Nb_4P_2 should lose a monomeric $[Nb(O_2)O_x]^{y-}$ unit after the condensation, which will require excess phosphate to reassemble to form Nb_6P_4 clusters.

Nb_6P_4 exhibits a bright yellow color both in solution and in the solid state. The yellow color of Nb_6P_4 is interesting because both Nb_4P_2 and peroxo-Nb_6 are colorless. The solution of **2** exhibits a peak at $\lambda = 325$ nm ($\varepsilon = 7500$) and a stronger ligand-to-metal charge-transfer (LMCT) band below $\lambda = 250$ nm (Figure 5). The peak at 325 nm tails to the high-energy limits of human vision, producing the yellow color. As the solution was titrated with base, the peak at $\lambda = 325$ nm blue shifted (Figure 5), suggesting a speciation change. The yellow color of the Nb_6P_4 solution fades as more TMAOH is added. The color change is immediate, but the speciation change is slower (hours), as discussed above. This result suggests that the color is more related to protonation, which is fast, rather than changes in speciation, which is much slower. Even the Nb_4P_2 solution becomes yellow after addition of phosphoric acid before the conversion to Nb_6P_4, which completes in hours, indicating that the yellow color is again likely due to protonation. We also note that previously known Keggin- or Dawson-type peroxoniobotungstate clusters exhibit a yellow color as well,[7] and those clusters are synthesized in acidic conditions and they consist of $Nb(O_2)$ groups. Thus both a $Nb(O_2)$ group and acidic conditions (protonation) are required for the yellow color. The loss of yellow color with increasing pH is likely to be due to deprotonation of the peroxoniobophosphate framework.

Using the Nb_6P_4 cluster as a precursor for the production of niobium phosphate films has been conducted by spin coating its solutions onto silicon substrates. As seen in Figure 6, a uniform amorphous film of $Nb_6P_4O_{25}$, exhibiting no pores or cracks, is readily realized. With a root-mean-square roughness

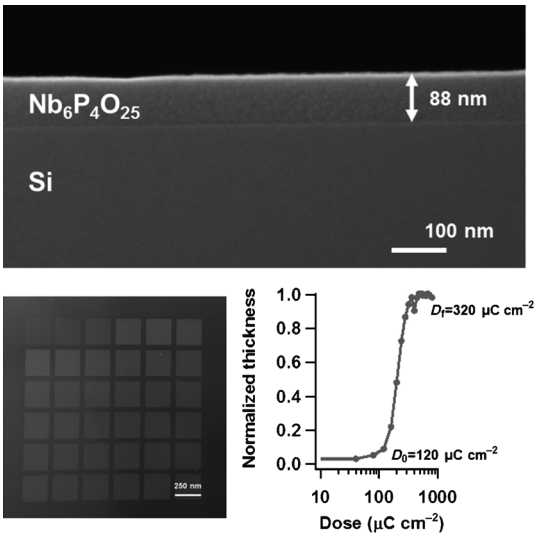

Figure 6. Cross-sectional SEM image of a spin-coated Nb_6P_4 solution (10 layers) on Si after annealing at 300 °C (top), SEM image of patterned film with increasing dose from 100 μC cm^{-2} by increment of 40 μC cm^{-2} (bottom left) and contrast curve following exposure with a 30 kV electron beam and water development (bottom right).

near 3 Å, the surface is nearly atomically smooth. The presence of phosphate inhibits crystallization to temperatures above 700 °C, which might be due to the formation of niobium phosphate glass. Crystalline Nb_2O_5 is found to separate into phases near 800 °C, followed by crystallization of Nb_9PO_{25} near 900 °C (Figure S9). To test patterning, the spin-coated film was exposed with a 30 kV electron beam to produce an array of exposed boxes at increasing dose. After exposure, the patterned structures were developed by dissolving the unexposed areas with water. The use of water instead of widely used TMAOH solution in the development step is more environmentally benign. As seen in Figure 6, the onset of insolubility begins with an exposure dose of $D_0 = 120$ μC cm^{-2} with complete gelation and insolubility occurring at a dose near $D_f = 320$ μC cm^{-2}. These dosage (sensitivity) values are comparable to those of the HafSOx films.[15] The calculated contrast value ($\gamma = (\log D_f - \log D_0)^{-1}$) from the curve is 2.3, which is in the lower range compared to other solution-processed, inorganic, patterned films.[1–5] The pattern formation in this study suggests that inter-cluster polymerization occurs via radiation-induced decomposition of peroxo groups and subsequent condensation like in the HafSOx system. In contrast, the Nb_4P_2 solution did not produce a patterned film—all the film was washed away during development—indicating that the film was not polymerized by irradiation. These results suggest that the smaller amount of TMA in Nb_6P_4 (three TMA per cluster) compared to Nb_4P_2 (five TMA per cluster) is more advantageous for electron-beam induced pattern formation. The TMA can sterically hinder the polymerization. This idea is supported by control experiments where the amount of TMA in the Nb_6P_4 solutions was augmented separately by adding TMAOH. In these experiments, dose increased and contrast decreased with TMA concentration.

In summary, we find that addition of peroxide and phosphate groups to aqueous Nb^V chemistry leads to two types of new peroxoniobophosphate clusters, the relative proportion of which depends on pH, including strongly acidic conditions. Switching between Nb_4P_2 and Nb_6P_4 clusters can be achieved by simple tuning of the pH. In addition, the Nb_6P_4 cluster enables the deposition of high-quality patterned thin films from simple aqueous solutions—a first step in evaluating their potential as functional materials for the semiconductor industry. Furthermore, these peroxoniobophosphate clusters have spurred the discovery and development of a rich new family of niobium phosphate glass, a subject of forthcoming contributions.

Experimental Section

Synthesis of 1: In a PTFE-lined autoclave (23 mL capacity), hydrous niobium oxide (3 g; 80% w/w) was mixed with TMAOH solution (8 mL, 25%), and then phosphoric acid (1 g, 85%) was added. The mixture was allowed to hydrothermally react at 130 °C for 16 h. A clear solution formed with pH 10.0. The product solution was diluted with water (ca. 10 mL), and then hydrogen peroxide solution (5 mL, 30%) was added slowly with stirring, and the solution pH was 6.5. The solution was evaporated at room temperature, and the crystalline product which formed after a few weeks was washed with ethanol on a frit. The product was recrystallized in methanol. Yield = 3.04 g (51%). Elemental analysis calcd (%) for $C_{20}H_{79}N_5Nb_4O_{31}P_2$: C 18.21, H 6.03, N 5.31, P 4.70, Nb 28.17; found: C 17.51, H 6.04, N 5.12, P 3.86, Nb 26.8.

Synthesis of 2: In a PTFE-lined autoclave (23 mL capacity), hydrous niobium oxide (5 g, 80% w/w) was mixed with TMAOH solution (7 mL, 25%). The mixture was allowed to hydrothermally react at 120 °C for 3 days. The solution contained mostly decaniobate after reaction, as checked with ESI-MS. The solution was washed with isopropanol in a centrifuge tube a few times until a sticky product remained. The product was dissolved in water (ca. 20 mL) and then hydrogen peroxide solution (5 mL, 30%) and phosphoric acid (2.5 mL, 85%) were added with stirring. The solution color became yellow after addition and the solution pH was 2.0. Bright yellow crystals formed during evaporation after half of the solution was evaporated at room temperature. The crystals were filtered on a frit and washed with water. More batches of crystals were harvested repeatedly during the evaporation of washed solution. Combined yield = 4.26 g (53%). Elemental analysis calcd (%) for $C_{12}H_{57}N_3Nb_6O_{43}P_4$: C 8.94, H 3.56, N 2.60, P 7.68, Nb 34.57; found: C 8.68, H 3.65, N 2.54, P 7.72, Nb 35.5.

Crystal data for $TMA_5[HNb_4P_2O_{14}(O_2)_4]\cdot 9H_2O$ (1): $C_{20}H_{79}N_5Nb_4O_{31}P_2$, $M = 1319.46$, triclinic, $a = 11.358(2)$, $b = 11.596(2)$, $c = 19.303(3)$ Å, $\alpha = 94.747(3)$, $\beta = 104.208(3)$, $\gamma = 99.452(3)^\circ$, $U = 2410.8(7)$ Å^3, $T = 93(2)$ K, space group $P\bar{1}$ (no.2), $Z = 2$, 28091 reflections measured, 10976 unique ($R_{int} = 0.0187$) which were used in all calculations. The final $wR(F^2)$ was 0.493 (all data).[16]

Crystal data for $TMA_3[H_7Nb_6P_4O_{24}(O_2)_6]\cdot 7H_2O$ (2): $C_{12}H_{55}N_3Nb_6O_{43}P_4$, $M = 1610.93$, triclinic, $a = 10.202(3)$, $b = 12.883(4)$, $c = 19.392(7)$ Å, $\alpha = 81.381(5)$, $\beta = 84.933(5)$, $\gamma = 68.635(4)^\circ$, $U = 2345.4(14)$ Å^3, $T = 88(2)$ K, space group $P\bar{1}$ (no.2), $Z = 2$, 30333 reflections measured, 10660 unique ($R_{int} = 0.0265$) which were used in all calculations. The final $wR(F^2)$ was 0.0773 (all data).[16]

Acknowledgements

This work was supported by an NSF CCI grant (CHE-1102637) in support of the Center for Sustainable Materials Chemistry. Additional support to J.H.S. was via a NSF-CHE-1310368 grant to W.H.C. We thank Shawn Decker for assistance with the electron-beam lithography. We thank Dr. Ping Yu and Corey Pilgrim for acquisition of solid-state and solution NMR spectra. We thank Peter Eschbach and Teresa Sawyer of the OSU Electron Microscopy Facility for assistance in the collection of SEM images.

Keywords: niobium · peroxides · phosphorus · polyoxometalates · synthesis

[1] A. E. Grigorescu, C. W. Hagen, *Nanotechnology* **2009**, *20*, 292001.
[2] B. Cardineau, R. Del Re, M. Marnell, H. Al-Mashat, M. Vockenhuber, Y. Ekinci, C. Sarma, D. A. Freedman, R. L. Brainard, *Microelec. Engineer.* **2014**, *127*, 44–50.
[3] E. Zanchetta, G. D. Giustina, G. Brusatin, *J. Appl. Phys.* **2014**, *116*, 103504.
[4] a) J. T. Anderson, C. L. Munsee, C. M. Hung, T. M. Phung, G. S. Herman, D. C. Johnson, J. F. Wager, D. A. Keszler, *Adv. Funct. Mater.* **2007**, *17*, 2117; b) A. Telecky, P. Xie, J. Stowers, A. Grenville, B. Smith, D. A. Keszler, *J. Vac. Sci. Technol. B* **2010**, *28*, C6S19–22; c) R. P. Oleksak, R. E. Ruther, F. Luo, K. C. Fairley, S. R. Decker, W. F. Stickle, D. W. Johnson, E. L. Garfunkel, G. S. Herman, D. A. Keszler, *ACS Appl. Mater. Interfaces* **2014**, *6*, 2917–2921.
[5] J. Stowers, D. A. Keszler, *Microelectron. Eng.* **2009**, *86*, 730.
[6] R. E. Ruther, B. M. Baker, J.-H. Son, W. H. Casey, M. Nyman, *Inorg. Chem.* **2014**, *53*, 4234–4242.
[7] a) D. A. Judd, Q. Chen, C. F. Campana, C. L. Hill, *J. Am. Chem. Soc.* **1997**, *119*, 5461–5462; b) M. K. Harrup, G.-S. Kim, H. Zeng, R. P. Johnson, D. VanDerveer, C. L. Hill, *Inorg. Chem.* **1998**, *37*, 5550–5556; c) G.-S. Kim, H. Zeng, W. A. Neiwert, J. J. Cowan, D. VanDerveer, C. L. Hill, I. A. Weinstock, *Inorg. Chem.* **2003**, *42*, 5537–5544; d) S.-J. Li, S.-X. Liu, C.-C. Li, F.-J. Ma, D.-D. Liang, W. Zhang, R.-K. Tan, Y.-Y. Zhang, L. Xu, *Chem. Eur. J.* **2010**, *16*, 13435–13442.
[8] a) N. Krishna Mohan, G. S. Baskaran, N. Veeraiah, *Phys. Status Solidi A* **2006**, *203*, 2083–2102; b) Z. Teixeira, O. L. Alves, I. O. Mazali, *J. Am. Ceram. Soc.* **2007**, *90*, 256–263; c) C. M. Chu, J. J. Wu, S. W. Yung, T. S. Chin, T. Zhang, F. B. Wu, *J. Non-Cryst. Solids* **2011**, *357*, 939–945; d) S. W. Yung, Y. S. Huang, Y.-M. Lee, Y. S. Lai, *RSC Adv.* **2013**, *3*, 21025–21032.
[9] D. Bayot, M. Devillers, *Coord. Chem. Rev.* **2006**, *250*, 2610–2626.
[10] H. Thomadaki, A. Lymberopoulou-Karaliota, A. Maniatakou, A. Scorilas, *J. Inorg. Biochem.* **2011**, *105*, 155–163.
[11] C. A. Ohlin, E. M. Villa, J. C. Fettinger, W. H. Casey, *Angew. Chem. Int. Ed.* **2008**, *47*, 8251–8254; *Angew. Chem.* **2008**, *120*, 8375–8378.
[12] C. A. Ohlin, E. M. Villa, J. C. Fettinger, W. H. Casey, *Inorg. Chim. Acta* **2010**, *363*, 4405–4407.
[13] Q. Geng, Q. Liu, P. Ma, J. Wang, J. Niu, *Dalton Trans.* **2014**, *43*, 9843–9846.
[14] a) T. M. Alam, M. Nyman, B. R. Cherry, J. M. Segall, L. E. Lybarger, *J. Am. Chem. Soc.* **2004**, *126*, 5610–5620; b) M. Nyman, T. M. Alam, F. Bonhomme, M. A. Rodriguez, C. S. Frazer, M. E. Welk, *J. Cluster Sci.* **2006**, *17*, 197–219.
[15] X. Thrun, K.-H. Choi, M. Freitag, A. Grenville, M. Gutsch, C. Hohle, J. K. Stowers, J. W. Bartha, *Microelectron. Eng.* **2012**, *98*, 226–229.
[16] CCDC-1034677 (**1**) and CCDC-1034678 (**2**) contain the supplementary crystallographic data for this paper. These data can be obtained free of charge from The Cambridge Crystallographic Data Centre via www.ccdc.cam.ac.uk/data_request/cif.

Received: February 17, 2015
Published online on March 13, 2015